# The Dipole Repeller

Y. Hoffman, D. Pomarède, R. Brent Tully, H. Courtois

# The Dipole Repeller

Yehuda Hoffman[1], Daniel Pomarède[2], R. Brent Tully[3] and Hélène Courtois[4]

*In accordance with Nature publication policy, this version is the original one submitted to Nature Astronomy. The accepted version is accessible online at Nature Astronomy and differs from this one. Nature Astronomy 2017, Volume 1 , article 36. We will be allowed to post in 6 months the accepted version on arxiv.*

[1]*Racah Institute of Physics, Hebrew University, Jerusalem 91904, Israel*

[2]*Institut de Recherche sur les Lois Fondamentales de l'Univers, CEA, Université Paris-Saclay, 91191 Gif-sur-Yvette, France*

[3]*Institute for Astronomy (IFA), University of Hawaii, 2680 Woodlawn Drive, HI 96822, USA*

[4]*University of Lyon; UCB Lyon 1/CNRS/IN2P3; IPN Lyon, France*

**In the standard ($\Lambda$CDM) model of cosmology the universe has emerged out of an early homogeneous and isotropic phase. Structure formation is associated with the growth of density irregularities and peculiar velocities. Our Local Group is moving with respect to the cosmic microwave background (CMB) with a velocity of $V_{\rm CMB} = 631 \pm 20$ km s$^{-1}$ [1] and participates in a bulk flow that extends out to distances of at least $\approx 20,000$ km s$^{-1}$ [2–4]. The quest for the sources of that motion has dominated cosmography since the discovery of the CMB dipole. The implicit assumption was that excesses in the abundance of galaxies induce the Local**

**Group motion[5–7]. Yet, underdense regions push as much as overdensities attract[8] but they are deficient of light and consequently difficult to chart. It was suggested a decade ago that an underdensity in the northern hemisphere roughly 15,000 $\mathrm{km\ s^{-1}}$ away is a significan factor in the local flow[9]. Here we report on kinematic evidence for such an underdensity. We map the large scale 3D velocity field using a Wiener filter reconstruction from the Cosmicflows-2 dataset of peculiar velocities, and identify the attractors and repellers that dominate the local dynamics. We show here that the local flow is dominated by a single attractor - associated with the Shapley Concentration - and a single previously unidentified repeller. Multipole expansion of the local flow provides further support for the existence and role played by the attractor and repeller. The bulk flow (i.e. dipole moment) is closely (anti)aligned with the repeller at a distance of $16,000 \pm 4,500$ $\mathrm{km\ s^{-1}}$. The expansion eigenvector of the shear tensor (i.e. quadrupole moment) is closely aligned with the Shapley Attractor out to ≈7,000 $\mathrm{km\ s^{-1}}$. The close alignment of the local bulk flow with the repeller provides further support for its dominant role in shaping the local flow. This Dipole Repeller is predicted to be associated with a void in the distribution of galaxies.**

The large scale structure of the universe is encoded in the flow field of galaxies. A detailed analysis of the flow uncovers the rich structure manifested by the distribution of galaxies, such as the prominent nearby clusters[10–13], the Laniakea supercluster[14] and the Arrowhead mini-supercluster[15]. A one-to-one correspondence between the observed density field, derived from redshift surveys, and the reconstructed 3D flow field has been established out to beyond 100 megaparsecs and down to a resolution of a few megaparsecs[13]. Yet, the flow contains more information

on distant structures from tides and from continuity across the zone obscured by the Galactic disk, the so-called Zone of Avoidance[11,16]. The Cosmicflows-2 dataset of peculiar velocities[17] provides reasonably dense coverage to $R \approx 10,000$ km s$^{-1}$ (distances are expressed in terms of their equivalent Hubble velocity).

However convergent features in the large scale flow patterns reveal important influences at $R \sim 16,000$ km s$^{-1}$ at the extremity of the data coverage.

The linear 3D velocity field is reconstructed here from the Cosmicflows-2 data by the Bayesian methodology of the Wiener Filter (WF) and constrained realizations (CRs; see Methods). The WF is a Bayesian estimator which assumes a prior model - here it is the $\Lambda$CDM model. It is a conservative estimator which balances between the data and its errors and the assumed prior model. Where the data is weak the WF estimation tends to the null hypothesis of a homogenous universe. The variance around the mean WF estimator is sampled by the CRs.

The WF is used to construct the cosmic velocity and the cosmic web. The web is defined here by the velocity shear tensor[18] - the web elements of the so-called V-web are defined by the number of eigenvalues of the tensor above a threshold value (see Methods). In the linear regime the flow is irrotational and constitutes a gradient of a scalar potential. Figure 1 shows the large scale structure out to a distance of 16,000 km s$^{-1}$. Three different aspects of the flow are depicted: streamlines which manifest the direction and magnitude of the velocity field (but do not represent trajectories; see Methods), red and grey surfaces present the knots and filaments of the V-web and the green-yellow surfaces correspond to the velocity potential.

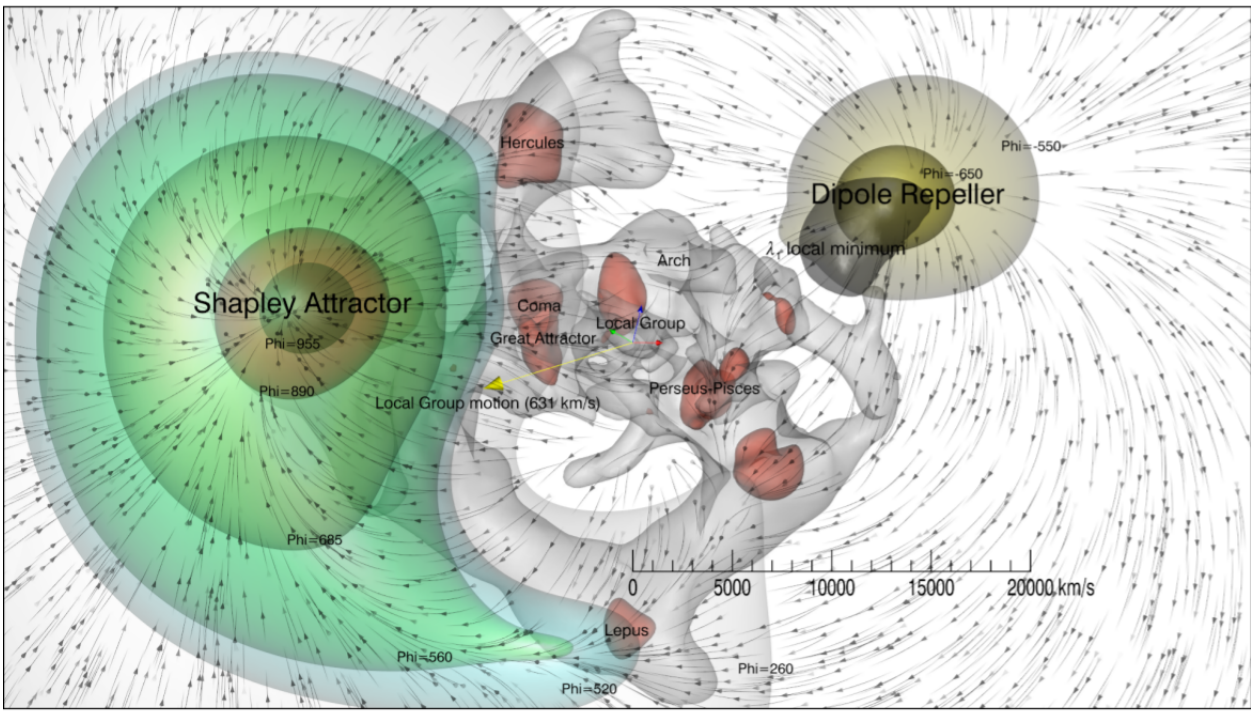


Figure 1: A face-on view of a slice 6,000 km $s^{-1}$ thick, normal to the directionn of the pointing vector $\hat{r} = (0.604, 0.720, -0.342)$. The scale can be inferred from the signpost made of three 2000 km/s-long arrows anchored at the origin of Supergalactic Coordinate System (SGX,SGY,SGZ), with Red, Green, Blue arrows associated with the SGX, SGY, SGZ axes, respectively. Three different elements of the flow are presented: mapping of the velocity field by means of streamlines (seeded randomly in the slice), red and grey surfaces present the knots and filaments of the V-web, respectively and equipotential surfaces are shown in green and yellow. The potential surfaces are enclosing the Dipole Repeller (in yellow) and the Shapley Attractor (in green) that dominate the flow. The yellow arrow indicates the direction of the CMB dipole ($gl = 276°$, $gb = 30°$).

Describing the gravitational dynamics in co-moving coordinates, by which the expansion of the universe is factored out, underdensities apply a repulsive force and overdensities an attractive one. We opt here to represent the vector field by means of streamlines - the tangent of which is in the direction of the velocity vector and its colour represents the amplitude of the vector. The sources and sinks of the streamlines are associated with the attractors and repellers of the large scale structure. These are closely associated with the voids and knots of the V-web. The voids (knots) are regions of diverging (converging) flow, namely regions where the Hessian of the velocity potential is negative (positive) definite, yet these regions are in general moving with respect to the CMB frame of reference. The repellers and attractors are stationary voids and knots (respectively), hence they correspond to local extrema of the gravitational potential. (See figure 1 and the on-line video for a visualization of the velocity potential.) Figure 2 shows a 3D visualization of the streamlines in a box of length 40,000 km $s^{-1}$ centered on the Local Group. The lines are seeded on a regular grid and extend either to converge with a knot or exit the box. All the flow lines of the left plot of figure 2 either converge onto an attractor located roughly at [$-$12,300, 7,400, $-$300] km $s^{-1}$ or cross out of the box. (Cartesian Supergalactic coordinates are assumed here.) The plot uncovers the existence of a repeller at the upper right hand side of the box - a region from which flow lines seem to diverge. Repellers are best manifested by the anti-flow, namely the negative of the velocity field. The right plot of figure 2 depicts the convergence of the streamlines of the anti-flow onto a repeller at [11,000, $-$6,000, 10,000] km $s^{-1}$. The WF reconstruction of the Cosmicflows-2 data detects a single attractor and a single repeller, the Shapley Attractor and the Dipole Repeller (hereafter the Attractor and the Repeller for brevity). (The accompanying video of the on-line version provides

a further visualization.)

The WF recovers the Attractor and the Repeller near the edge of the Cosmicflows-2 data. It is the long range correlation of the velocity field that renders the imprint of the Repeller and the Attractor on the local flow. Multipole expansion provides a different insight into the nature of the local flow. Here the spherical top-hat weighted bulk flow (i.e. dipole) and shear tensor (i.e. quadrupole moments) are evaluated at variable radius $R$[11, 16, 19, 20]. A single attractor or repeller induces a dipole and the expansion eigenvector of the shear tensor aligned with its direction and a degeneracy of the other two eigenvalues/eigenvectors. This is the telltale signature a single dominant attractor or repeller. The local flow is not dominated by a single attractor or repeller. In the following we emphasize the directional aspects of the dipole and shear eigenvectors. The WF acts as an adaptive filter - where data is missing and/or noisy it suppresses more strongly the signal and the small scale structure. Hence the contribution of the (better sampled) Attractor cannot be directly compared with the (extremely poorly sampled) Repeller. Yet, directions are robustly recovered by the WF. Figure 3 presents an aitoff projection of the following directions: 1. the Repeller; 2. the Attractor; 3. the CMB dipole and its anti-apex; 4. the bulk velocity of top-hat spheres of $R = (2,000, 3,000, ..., 15,000)$ km s$^{-1}$, $\mathbf{V}_{\rm bulk}$(R), of the WF reconstructed flow field; 5. the three eigenvectors of the shear tensor ($\hat{\mathbf{e}}_i$, i=1,2,3) of the WF field. The figure shows the strong anti-alignment of the CMB dipole and the bulk velocity of spheres of radii smaller than 15,000 km s$^{-1}$ with the Repeller. Beyond that radius the bulk velocity looses its coherence in terms of direction, as the scatter in direction steadily increases. The third eigenvector of the shear tensor ($\hat{\mathbf{e}}_3$), that reflects the direction of maximal expansion, is aligned with the direction of the Attractor

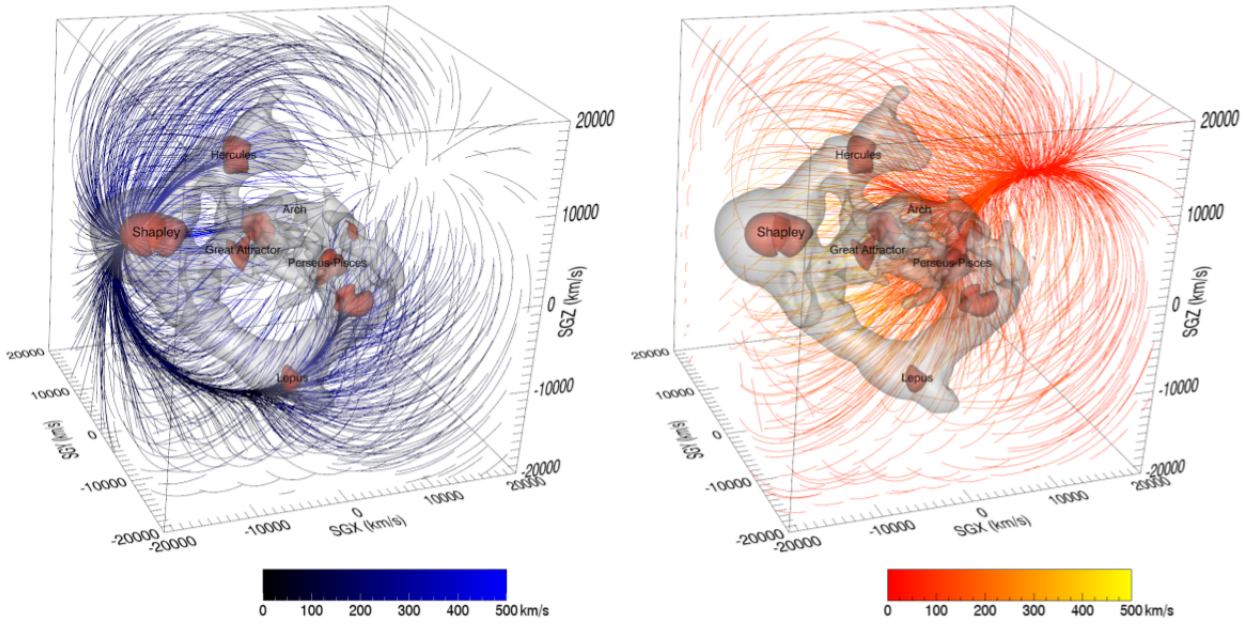


Figure 2: A three dimensional (3D) view of the stream lines of the flow field (in black-blue, left panel) and of the anti-flow (in yellow-red, right panel). The stream lines are seeded on a regular grid and are coloured according to the magnitude of the velocity, The flow stream lines clearly diverge from the Repeller and converge on the Attractor. For the anti-flow the divergence and convergence are switching roles. The knots and filaments of the V-web are shown for reference. (For a 3D view look at the accompanying video, 00:56 - 01:28.)

out to $R = 7,000$ km s$^{-1}$. Figure 4 further presents the mean and the scatter around the cosine of the angles formed between the bulk velocity and the Repeller, $\mu_{\rm bulk}(R) = \cos(\mathbf{V}_{\rm bulk}, \mathbf{R}_{\rm GR})$, and between $\hat{\mathbf{e}}_3$ and the Attractor, $\mu_{\rm e3}(R) = \cos(\hat{\mathbf{e}}_3(R), \mathbf{R}_{\rm Shapley})$.

The close alignment of the bulk velocity with the Repeller out to roughly $R = 16,000$ km s$^{-1}$, where $\mu_{\rm bulk}(R) = -0.96 \pm 0.042$, provides the strongest support for the validity of the Repeller and for its dominant role in dictating the local flow. It is interesting to study the shear tensor. The expansion eigenvector is closely aligned with the direction to the Shapley Attractor out to $R \approx 7,000$ km s$^{-1}$ - a direction which coincides with the Great Attractor, located at the bottom of the Laniakea basin of attraction[14] at (-4,700, 1,300, 500) km s$^{-1}$. It is the combined mass distribution within the Laniakea and Shapley superclusters that dominates the tidal field - with the inverse cubic distance dependence of the tidal interaction tipping the balance towards the Laniakea/Great Attractor.

The main findings of the article are tested against statistical and systematic uncertainties. There is no doubt about the existence of the Shapley Concentration and therefore we focus our attention mostly on the Repeller. The strong support for the existence of the Repeller comes not only from its close alignment of the bulk velocity but also the small scatter around the mean WF value, $\mu_{\rm bulk}(R) = -0.96 \pm 0.04$ for $R \approx 16,000$ km s$^{-1}$ (figure 4). Assuming that the Repeller is the dominant structure that determines the direction of the bulk flow the scatter in $\mu_{\rm bulk}(R)$ can be translated to uncertainty in the position of the Repeller, $\Delta R_{\rm GR} \approx 4,500$ km s$^{-1}$ (see Methods). Next, a possible 'edge of the data' effect is considered, driven by the concern that both the Attractor

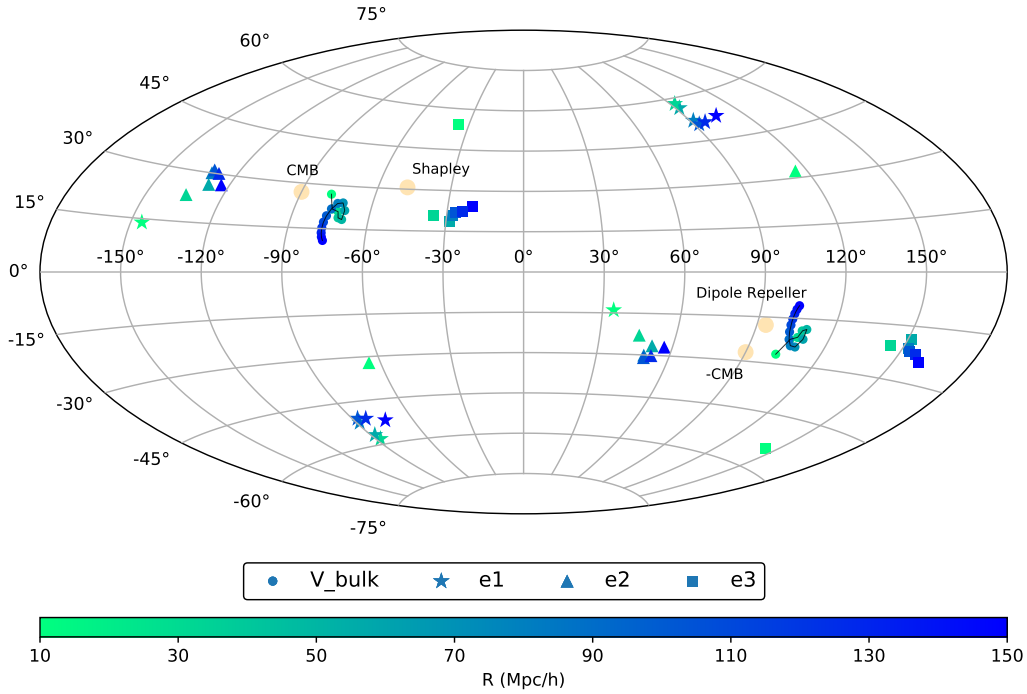


Figure 3: Aitoff projection in galactic coordinates of the principal structures and directions that characterize the flow: the Dipole Repeller (GR), the Shapley Attractor, the CMB dipole, the bulk velocity and the three eigenvectors of the velocity shear tensor. The latter two quantities are evaluated across spheres of radii ranging up to 30,000 km $s^{-1}$ for the bulk velocity and 15,000 km $s^{-1}$ for the eigenvectors. The close (anti)alignment of the bulk velocity and the alignment of the $\hat{e}_3$ eigenvector with the Attractor are robustly manifested.

and the Repeller are located at the extremity of the Cosmicflows-2 data zone. This issue has been addressed by restricting the full Cosmicflows data to spheres of radii 6,000, 8,000 and 10,000 km $s^{-1}$ which contain 49%, 67% and 82% of the full data, respectively. The WF applied to these subsets of data recovers the Repeller to within roughly $\Delta R_{\rm GR}$. Systematic errors, such as the ones introduce by the Malmquist bias, can introduce systematic in- or outflows but the validity of the proposed morphology is supported by the reconstructed back outflow from the Repeller.

The general picture that emerges here is of a complex flow that cannot be explained by a simple toy model, yet the main structures that shape the local flow can be identified. The WF finds that the flow is dominated by a single attractor and a single repeller. The dominance of the Repeller is manifested by the fact that the CMB and the bulk velocity dipoles are all strongly (anti)aligned with its direction. The Repeller pushes our local patch of the universe. The Repeller dominates the bulk flow out to a distance of 16,000 $\pm$ 4,500 km $s^{-1}$and the Attractor dominates the shear term out to roughly 7,000 km $s^{-1}$. In the language of multipole expansion the repeller dominates the dipole and the attractor dominates the quadrupole moments. The role played by the Shapley Attractor is not surprising - the earlier findings on influences beyond the Great Attractor[6,7,9,21,22] suggested it. The existence of the Repeller was only very vaguely hinted before. A study of the all-sky distribution of X-ray selected clusters uncovered a significant under-density of clusters in the northern hemisphere roughly 15,000 km $s^{-1}$ away[9]. It suggested that this under-density may be as significant as the overdensity of clusters in the southern hemisphere in inducing the local flow. Earlier examinations of galaxy peculiar velocities found a north-south anisotropy in (galactic) y-component of the velocities[3] and that the sources responsible for the bulk flow are at an effective

distance >30,000 km $s^{-1}$ [20]. Here, the source of the repulsion is identified for the first time. Arguably, the dominance of the Dipole Repeller over the Shapley Attractor is the main novel and surprising finding of this study. The predicted position of the Repeller is in a region that is yet poorly covered by existing redshift surveys. We predict the Repeller to be associated with a void in the distribution of galaxies.

In the linear regime of gravitational instability repellers are as abundant and dominant as attractors. Yet observationally, repellers are much harder to identify than attractors. The association of repellers with underdensities renders them strongly deficient of galaxies, in general, and clusters of galaxies, in particular. The detection of voids by means of redshift surveys is challenging. Our use of peculiar velocities as tracers of the large scale structure overcomes that observational hindrance and unveils the existence of the new structure we call the Dipole Repeller.

## 1 methods

**Cosmicflows-2 dataset:** The present studies is based on the second release catalogue of galaxy distances and peculiar velocities, Cosmicflows-2 [17], that extends sparsely to recession velocities of 30,000 km $s^{-1}$ (redshift $z \approx 0.1$). It consists of 8,161 entries with high density of coverage inside 10,000 km $s^{-1}$. Here we used a grouped version of the Cosmicflows-2 data, in which all galaxies forming a group, of two or more, are merged to one data entry. The grouped Cosmicflows-2 data consists of 4885 entries. Six methodologies are used for distance estimation: Cepheid star pulsations, the luminosity terminus of stars at the tip of the red giant branch, surface brightness

fluctuations of the ensemble of stars in elliptical galaxies, type Ia supernovae, the fundamental plane in luminosity, radius, and velocity dispersion of elliptical galaxies, and the Tully-Fisher correlation between the luminosities and rotation rates of spiral galaxies.

**Wiener filter and Constrained Realizations:** In the standard model of cosmology the linear velocity field constitutes a Gaussian random vector field[23]. The Cosmicflows-2 dataset, as all other available velocity surveys, provides a sparse, incomplete, inhomogeneous and a very noisy sampling of the local flow. The Bayesian formalism of the WF and CRs provides the optimal methodology for the reconstruction (estimation) of the underlying velocity field and the associated uncertainties in the linear regime[11,24–26]. The WF/CRs reconstruction is based on an assumed prior cosmological model - the $\Lambda$CDM model with the WMAP inferred cosmological parameters. The current WF and CR fields are the ones reported in our bulk velocity article[4]. The results presented here are insensitive to the exact values of the $\Lambda$CDM parameters, in particular to the differences between the WMAP and Planck parameters.

**Cosmic V-web:** The cosmic web is defined here by the means of the V-web[18]. The V-web is a mathematical model used to construct the cosmic web. The model starts with the continuous velocity field and the velocity shear tensor evaluated for that field (equation 1). Consider a given point in space at which the shear tensor is evaluated, and thereby its eigenvalues and eigenvectors. The so-called V-web is defined by a threshold values ($\lambda_{\rm th}$) - a free parameter which defines the web. The number of eigenvalues above $\lambda_{\rm th}$ defines the web classification at that point - 0, 1, 2 or 3 corresponds to the point being a void, sheet, filament or knot. The normalized velocity shear

tensor at a given grid cell, is defined by:

$$\Sigma_{\alpha\beta} = -\frac{1}{2H_0}(\partial_\alpha v_\beta + \partial_\beta v_\alpha) \tag{1}$$

The standard definition of the velocity shear tensor is modified here by the Hubble constant ($H_0$) normalization, which makes it dimensionless. The minus sign is introduced so that a positive eigenvalue corresponds to a contraction. Eigenvalues are ordered by decreasing value, which implied that $\hat{e}_1$ points in the direction of maximum collapse and $\hat{e}_3$ points toward maximum expansion. The V-web is defined by the effective resolution of the velocity field and by the value of the threshold. Here a Gaussian smoothing of $R_s = 250$ km s$^{-1}$ and $\lambda_{\rm th} = 0.04$ are assumed.

**Multipole expansion of the flow:** A first order expansion of a potential (i.e. irrotational) velocity field, $\vec{v}(\vec{r})$, around a point labeled by $\mathbf{0}$ yields,

$$v_\alpha(\vec{r}) \sim v_{0,\alpha} + (\partial_\beta\, v_\alpha)\, r_\beta = v_{0,\alpha} - H_0\, \Sigma_{\alpha\beta}\, r_\beta, \tag{2}$$

where $v_{0,\alpha}$ and $\Sigma_{\alpha\beta}$ are evaluated at the point $\mathbf{0}$. This expansion is equivalent to a dipole and quadrupole expansion of the (velocity) potential. The flow in a sphere of radius $R$ is modelled here as the sum of a bulk flow, $\mathbf{V}_{\rm bulk}(R)$, and a shear term, $\Sigma_{\alpha\beta}(R)$, in the manner of equation 2. The parameters of the model, i.e. the bulk velocity vector and the symmetric tensor, are found by minimizing the quadratic residual between the model and the actual velocity field, with a spherical top-hat window function weighting.

**Streamlines:** In the linear regime the flow is irrotational, namely it is a potential flow, and hence the velocity field can be written as a gradient of a scalar (velocity) potential, $\vec{v} = \nabla\phi_v(\vec{r})$.

In this linear regime the peculiar velocity ($\vec{u}$) and gravitational field ($\vec{g}$) are simply related by $\vec{u} = \frac{2}{3}\frac{f(\Omega_m,\Omega_\Lambda)}{H\Omega_m}\vec{g}$ where $\Omega_m, \Omega_\Lambda$ and $H$ are the time dependent cosmological matter and dark energy density parameters and Hubble's constant, respectively. The velocity and gravitational potential are similarly related. Inspired by the similarity between the gravitational potential in linear theory, hence also the velocity potential, to the electrical potential in electro-statistics, we present the flow field by field lines which we call here stream or flow lines. A trajectory of a streamline, $\vec{l}(s)$ where $s$ is the line parameter, is calculated by integrating the line equation, $d\vec{r}(s) = \vec{v}(\vec{r}(s))ds$. The numerical calculation of a streamline involves the determination of the seeds of the stream lines and the number of integration steps. For small number of integrations steps and a regular grid of seeds the streamlines resemble velocity arrows. For a large number of steps the flow and anti-flow lines are either trapped by attractors or repellers or leave the box. It should be emphasized here that the streamlines are a graphical mean for the presentation of a vector field and do not represent trajectories of objects.

**Video:** The video (http://vimeo.com/pomarede/dipolerepeller or http://irfu.cea.fr/dipolerepeller) commences with the presentation of the large scale structure by means of the surfaces that define the filaments and knots of the V-web. The motion of the Local Group with respect to the CMB is displayed by a yellow arrow. The growth of streamlines through integration steps from a regular array of seeds are illustrated. The fully developed streamlines clearly shows a pattern dominated by a single repeller and a single attractor. The growth of the streamlines of the anti-flow is shown in a similar manner - the anti-flow is being repelled by the Attractor and attracted by the Repeller. A different presentation of the flow and anti-flow streamlines is obtained by confining the seeds of

the flow lines to the neighbourhood of the Repeller (in blue-black) and those of the anti-flow to the vicinity of the Attractor (in orange-red). The attractive flow develops mainly in a plane containing the major over-densities: Perseus-Pisces, Lepus and Hercules. The repulsive anti-flow develops in the orthogonal plane that corresponds roughly to the supergalactic equator. The video reveals the almost exact alignment of the Local Group velocity vector with the Dipole Repeller and the much poorer alignment with the Shapley Attractor. The Repeller and Attractor constitute local maxima and minima of the gravitational potential.

**Uncertainties assessment:** The probability distribution of the alignment of the bulk velocity and the eigenvectors of the shear tensor is sampled by means of an ensemble of 20 CRs, constrained by the Cosmicflows-2 data and evaluated within the WMAP parameters of the $\Lambda$CDM model. The CRs are evaluated on a grid of size $256^3$ spanning a box of 256,000 km s$^{-1}$ on its side. The bulk velocity and the velocity shear tensor are obtained by a convolution of the velocity field with a spherical top-hat window of radius $R$ and are evaluated at the center of the box, i.e. the location of the Local Group. Figure 4 presents the alignment of the bulk velocity and the 3rd eigenvector of the shear tensor with the Repeller and the Attractor respectively over a range of radii of $R = (2,000, 3,000, ...30,000)$ km s$^{-1}$. The uncertainty in $\mu_{\rm bulk}(R)$ is used to assess the uncertainty in the position of the Repeller. At $R \approx 16,000$ km s$^{-1}$ we find $\mu_{\rm bulk}(R) = -0.96 \pm 0.04$. Assuming the Repeller to be responsible for the direction of the bulk velocity the uncertainty in $\mu_{\rm bulk}$ is translated to a projected distance (at a distance of 16,000 km s$^{-1}$) we find $\Delta R_{\rm GR} \approx 4,500$ km s$^{-1}$. The uncertainty in $\mu_{\rm bulk}$ changes significantly over the range $R =$ 11,000 to 20,000 km s$^{-1}$. This again translates to an uncertainty in the radial position of roughly 4,500 km s$^{-1}$.

Next a possible 'edge of the data' systematic effect is considered. To meet this end the full Cosmicflows data has been trimmed in spheres of radii 6,000, 8,000 and 10,000 km $s^{-1}$ which contain 49%, 67% and 82% of the full data, respectively. The WF has been applied to these subsets of data and the resulting (anti)flow field has been compared with that of the full data (figure 5). The overall structure of the flow fields of the subsamples follow that of the full Cosmicflows-2 data. The anti-flow converges into two repellers in the 6,000 km $s^{-1}$ case and into single repellers for the 8,000 and 10,000 km $s^{-1}$ cases. Table 1 provides the location and distances from the Local Group and the Repeller for each case. It also provides the fraction of data contained in the each subsample. It is remarkable that with less than half the data (6,000 km $s^{-1}$ case) the WF recovers the general (anti)flow towards the general position of the Repeller. Taking the mean position of the two repellers it is found to be a mere 2,500 km $s^{-1}$ from the Repeller. Single repellers are found for the larger subsamples that consist of 67% and 82% of the data at distances of 4,300 and 500 km $s^{-1}$ from the Repeller, respectively. We conclude that the Repeller is not a fictitious structure induced by an 'edge of the data' effect.

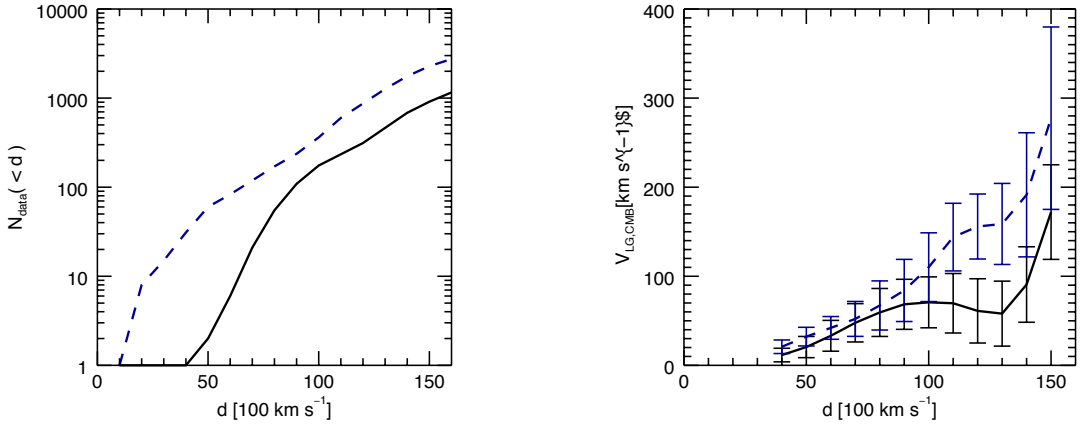


Figure 4: Alignment of the bulk velocity with the direction of the Repeller in the lower set of curves and of the $\hat{e}_3$ eigenvector with the Attractor in the upper set of curves. The alignment is presented by the mean (solid lines) and the mean $\pm$ standard deviation (dashed lines), where the statistics are calculated over an ensemble of 20 constrained realizations. The alignment with the Attractor is expressed by $\mu_{\rm e1}(R)$ (upper curve) and with the Repeller by $\mu_{\rm bulk}(R)$ (lower curve). The downward black arrow and the upward blue arrow indicate the distances of the Repeller and the Attractor, respectively, from the Local Group.

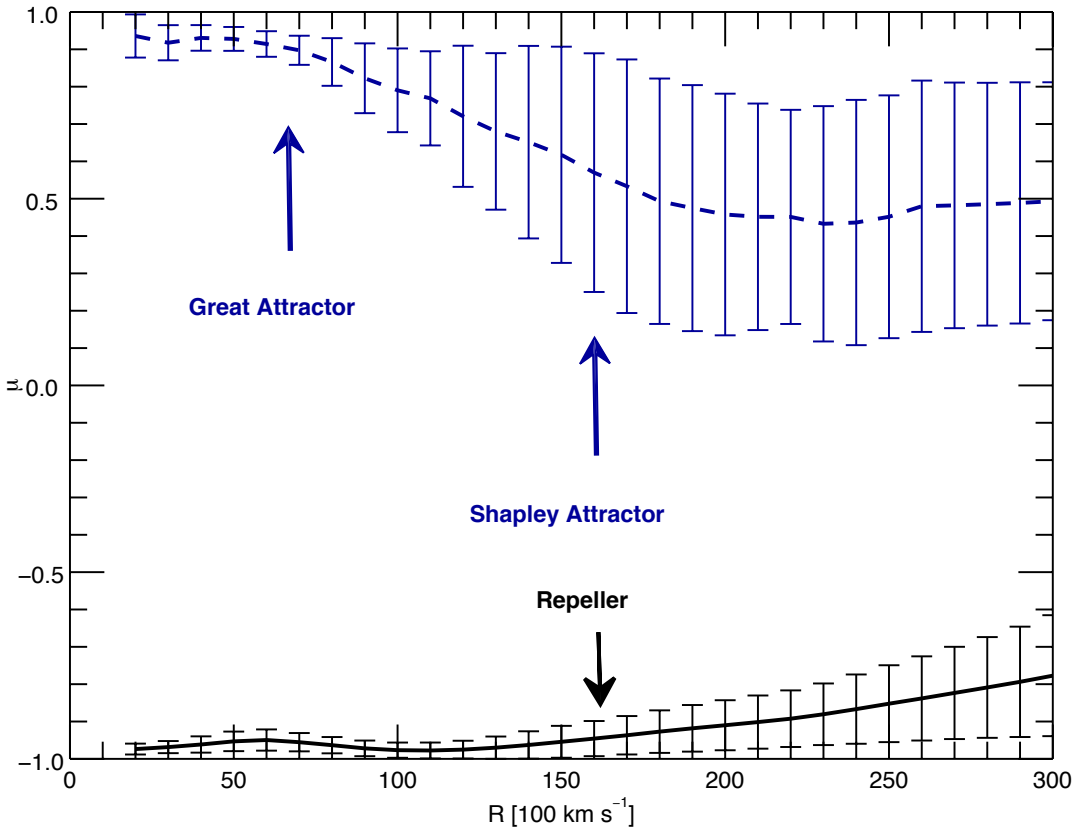


Figure 5: The anti-flow streamlines of the WF reconstruction of the three trimmed Cosmicflows-2 data: The $R = 6,000$ (left panel), $8,000$ (middle panel) and $10,000$˜km s$^{-1}$(right panel). These plots need to be compared with the equivalent plot made out of the full dataset (right panel of figure 2). In the case of the shallowest data ($R = 6,000$ km s$^{-1}$) the repeller breaks into two separate repellers. For the other datasets the flow convergence to a single repeller. Table 1 presents the location of the repellers of the sub-sample, their distances from the Local Group and from the Repeller.

| distance cut [$\mathrm{km\ s^{-1}}$] | % of data | [SGX, SGY, SGZ] [$\mathrm{km\ s^{-1}}$] | R [$\mathrm{km\ s^{-1}}$] | $d_{GR}$ [$\mathrm{km\ s^{-1}}$] |
|---|---|---|---|---|
| 6,000 | 49 | [12,500, 2,600, 9,800] | 16,100 | 8,700 |
| | | [10,000, -11,600, 10,500] | 18,500 | 5,700 |
| 8,000 | 67 | [10,600, -5,800, 10,000] | 13,700 | 4,300 |
| 10,000 | 82 | [10,900, -2,100, 8,100] | 15,600 | 500 |
| full | 100 | [11,000, -6,000, 10,000] | 16,000 | 0 |

Table 1: Cosmicflows-2 subsamples: The location, distance ($R$) and the distance from the Repeller ($d_{GR}$) of the repeller found for the different distance cuts of the data (first column). Two repellers are identified for the 6,000 $\mathrm{km\ s^{-1}}$ subsample and the first two raws present their locations and distances. The mean position of these two repellers is located at a distance of $d_{GR}$=2,500 $\mathrm{km\ s^{-1}}$.

1. Fixsen, D. J. *et al.* The Cosmic Microwave Background Spectrum from the Full COBE FIRAS Data Set. *ApJ* **473**, 576 (1996). arXiv:astro-ph/9605054.

2. Nusser, A. & Davis, M. The Cosmological Bulk Flow: Consistency with ΛCDM and z ≈ 0 Constraints on $\sigma_8$ and $\gamma$. *ApJ* **736**, 93 (2011). 1101.1650.

3. Watkins, R. & Feldman, H. A. Large-scale bulk flows from the Cosmicflows-2 catalogue. *MNRAS* **447**, 132–139 (2015). 1407.6940.

4. Hoffman, Y., Courtois, H. M. & Tully, R. B. Cosmic bulk flow and the local motion from Cosmicflows-2. *MNRAS* **449**, 4494–4505 (2015). 1503.05422.

5. Lilje, P. B., Yahil, A. & Jones, B. J. T. The tidal velocity field in the Local Supercluster. *ApJ* **307**, 91–96 (1986).

6. Lynden-Bell, D. *et al.* Spectroscopy and photometry of elliptical galaxies. V - Galaxy streaming toward the new supergalactic center. *ApJ* **326**, 19–49 (1988).

7. Dressler, A. The Great Attractor - Do galaxies trace the large-scale mass distribution? *Nature* **350**, 391–397 (1991).

8. Lahav, O., Lynden-Bell, D. & Rowan-Robinson, M. The peculiar acceleration of the Local Group as deduced from the optical and IRAS flux dipoles. *MNRAS* **234**, 677–701 (1988).

9. Kocevski, D. D. & Ebeling, H. On the Origin of the Local Group's Peculiar Velocity. *ApJ* **645**, 1043–1053 (2006). astro-ph/0510106.

10. Dekel, A., Bertschinger, E. & Faber, S. M. Potential, velocity, and density fields from sparse and noisy redshift-distance samples - Method. *ApJ* **364**, 349–369 (1990).

11. Zaroubi, S., Hoffman, Y. & Dekel, A. Wiener Reconstruction of Large-Scale Structure from Peculiar Velocities. *ApJ* **520**, 413–425 (1999). arXiv:astro-ph/9810279.

12. Courtois, H. M., Hoffman, Y., Tully, R. B. & Gottlöber, S. Three-dimensional Velocity and Density Reconstructions of the Local Universe with Cosmicflows-1. *ApJ* **744**, 43 (2012). 1109.3856.

13. Courtois, H. M., Pomarède, D., Tully, R. B., Hoffman, Y. & Courtois, D. Cosmography of the Local Universe. *AJ* **146**, 69 (2013). 1306.0091.

14. Tully, R. B., Courtois, H., Hoffman, Y. & Pomarède, D. The Laniakea supercluster of galaxies. *Nature* **513**, 71–73 (2014). 1409.0880.

15. Pomarède, D., Tully, R. B., Hoffman, Y. & Courtois, H. M. The Arrowhead Mini-supercluster of Galaxies. *ApJ* **812**, 17 (2015). 1509.02622.

16. Hoffman, Y., Eldar, A., Zaroubi, S. & Dekel, A. The Large-Scale Tidal Velocity Field. *ArXiv Astrophysics e-prints* (2001). astro-ph/0102190.

17. Tully, R. B. *et al.* Cosmicflows-2: The Data. *AJ* **146**, 86 (2013). 1307.7213.

18. Hoffman, Y. *et al.* A kinematic classification of the cosmic web. *MNRAS* **425**, 2049–2057 (2012). 1201.3367.

19. Jaffe, A. H. & Kaiser, N. Likelihood Analysis of Large-Scale Flows. *ApJ* **455**, 26 (1995). astro-ph/9408046.

20. Feldman, H. A., Watkins, R. & Hudson, M. J. Cosmic flows on 100 $h^{-1}$ Mpc scales: standardized minimum variance bulk flow, shear and octupole moments. *MNRAS* **407**, 2328–2338 (2010). 0911.5516.

21. Scaramella, R., Baiesi-Pillastrini, G., Chincarini, G., Vettolani, G. & Zamorani, G. A marked concentration of galaxy clusters - Is this the origin of large-scale motions? *Nature* **338**, 562–564 (1989).

22. Raychaudhury, S. The distribution of galaxies in the direction of the 'Great Attractor'. *Nature* **342**, 251–255 (1989).

23. Peebles, P. J. E. *The large-scale structure of the universe* (1980).

24. Hoffman, Y. & Ribak, E. Constrained realizations of Gaussian fields - A simple algorithm. *ApJL* **380**, L5–L8 (1991).

25. Hoffman, Y. Gaussian Fields and Constrained Simulations of the Large-Scale Structure. In Martínez, V. J., Saar, E., Martínez-González, E. & Pons-Bordería, M.-J. (eds.) *Data Analysis in Cosmology*, vol. 665 of *Lecture Notes in Physics, Berlin Springer Verlag*, 565–583 (2009).

26. Zaroubi, S., Hoffman, Y., Fisher, K. B. & Lahav, O. Wiener Reconstruction of the Large-Scale Structure. *ApJ* **449**, 446 (1995). arXiv:astro-ph/9410080.

Acknowledgments : Jenny Sorce and Stefan Gottloeber are gratefully acknowledged for valuable discussions and Alexandra Dupuy for her help in preparing Figure 3. We express our gratitude to K. Bowles and S. Thompson for the narration in the supplementary video. Support has been provided by the Israel Science Foundation (1013/12), the Institut Universitaire de France, the US National Science Foundation, Space Telescope Science Institute for observations with Hubble Space Telescope, the Jet Propulsion Lab for observations with Spitzer Space Telescope and NASA for analysis of data from the Wide-field Infrared Survey Explorer.

Support has been provided by the Israel Science Foundation (1013/12), the Institut Universitaire de France, the US National Science Foundation, Space Telescope Science Institute for observations with Hubble Space Telescope, the Jet Propulsion Lab for observations with Spitzer Space Telescope and NASA for analysis of data from the Wide-field Infrared Survey Explorer. The authors declare that they have no competing financial interests. Correspondence and requests for materials should be addressed to Y.H. (email: hoffman@huji.ac.il).

**Data availability statement.** The data that support the plots within this paper and other findings of this study are available from the corresponding author upon reasonable request. It is also available freely at the Extragalactic Distance Database: edd.ifa.hawaii.edu and through the NED interface. Use of the data and flow model must cite this article.